J. Fluid Mech. (2013), *vol.* 722, *pp.* 291–316.
doi:10.1017/jfm.2013.93

Dynamics and stability of the wake behind tandem cylinders sliding along a wall

A. Rao[1], M. C. Thompson[1], T. Leweke[2,†] and K. Hourigan[1,3]

[1]Fluids Laboratory for Aeronautical and Industrial Research (FLAIR), Department of Mechanical and Aerospace Engineering, Monash University, Melbourne, Victoria 3800, Australia

[2]Institut de Recherche sur les Phénomènes Hors Équilibre (IRPHE), UMR 7342 CNRS, Aix-Marseille Université, 13384 Marseille, France

[3]Division of Biological Engineering, Monash University, Melbourne, Victoria 3800, Australia

(Received 4 July 2012; revised 10 December 2012; accepted 11 February 2013)

The dynamics and stability of the flow past two cylinders sliding along a wall in a tandem configuration is studied numerically for Reynolds numbers (Re) between 20 and 200, and streamwise separation distances between 0.1 and 10 cylinder diameters. For cylinders at close separations, the onset of unsteady two-dimensional flow is delayed to higher Re compared with the case of a single sliding cylinder, while at larger separations, this transition occurs earlier. For Reynolds numbers above the threshold, shedding from both cylinders is periodic and locked. At intermediate separation distances, the wake frequency shifts to the subharmonic of the leading-cylinder shedding frequency, which appears to be due to a feedback cycle, whereby shed leading-cylinder vortices interact strongly with the downstream cylinder to influence subsequent leading-cylinder shedding two cycles later. In addition to the shedding frequency, the drag coefficients for the two cylinders are determined for both the steady and unsteady regimes. The three-dimensional stability of the flow is also investigated. It is found that, when increasing the Reynolds number at intermediate separations, an initial three-dimensional instability develops, which disappears at higher Re. The new two-dimensional steady flow again becomes unstable, but with a different three-dimensional instability mode. At very close spacings, when the two cylinders are effectively seen by the flow as a single body, and at very large spacings, when the cylinders form independent wakes, the flow characteristics are similar to those of a single cylinder sliding along a wall.

Key words: wakes, vortex shedding, instability

1. Introduction

The wakes behind generic bluff bodies such as cylinders and spheres placed in a free stream have been widely investigated. Several reviews (e.g. Williamson 1996; Norberg 2003) provide a comprehensive picture of the flow dynamics in the laminar and turbulent regimes, obtained both experimentally and numerically. For Reynolds numbers (Re, based on the cylinder diameter D and free stream velocity U) below 47, the wake is steady. Above this value, and up to $Re \simeq 180$, laminar vortex shedding

† Email address for correspondence: thomas.leweke@irphe.univ-mrs.fr

is observed, which, in the absence of end effects, is periodic and two-dimensional. The three-dimensional transition regime, found in the range $180 \lesssim Re \lesssim 300$, was first described in detail by Williamson (1988). The initial three-dimensional shedding mode (mode A) involves a spanwise waviness of the shed vortices, with a wavelength of approximately four cylinder diameters, and a discontinuity in the evolution of the shedding frequency. It can be related to an elliptic instability of the vortex cores (Thompson, Leweke & Williamson 2001). A second mode (mode B) appears at higher Reynolds numbers ($Re \gtrsim 230$), with a smaller spanwise wavelength of approximately one diameter. It involves the amplification of secondary streamwise vortices in the strain-dominated braid regions between the shed vortices. Initially, the two modes co-exist, with a subsequent gradual shift to a pure mode B, accompanied by a second discontinuity in the frequency relation. The characteristics of the two instability modes, including the associated vortex structures, were documented numerically by a number of authors (Mittal & Balachandar 1995; Zhang *et al.* 1995; Barkley & Henderson 1996; Thompson, Hourigan & Sheridan 1996; Henderson 1997).

The presence of a second bluff body of similar dimensions in close proximity influences the wakes behind each body, and also the forces experienced by each one of them. Critical parameters for categorizing the flow regimes for a particular Reynolds number include the separation distance and the magnitudes of lift and drag forces experienced by the cylinders. Biermann & Herrnstein (1933), in their investigation of streamlined struts and cylinders, found that the drag on the upstream cylinder is not greatly influenced by the presence of the downstream cylinder, however the drag on the rear cylinder was greatly reduced by the upstream cylinder. They also found that the wake from the upstream cylinder was not fully developed in the presence of another body at close separation distances. Igarashi (1981) carried out an experimental study for cylinders in a tandem configuration at $Re \simeq 10^4$ and classified the flow based on the separation distance. A similar study was conducted by Zdravkovich (1987), who recorded the force variations for cylindrical arrays of tubes in various configurations such as in-line, side by side and staggered. The broad classification based on the normalized longitudinal separation distance S/D (see figure 1) is as follows (note that some authors use the centre-to-centre longitudinal separation instead of the spacing between the cylinders).

(a) A regime of close spacing, $0.1 \leqslant S/D \leqslant 0.2$–$0.8$, where the shear layers shed from the upstream cylinder do not reattach to the downstream cylinder. The two cylinders behave as a single extended body and vortices are formed from the detached shear layers of the downstream cylinder.

(b) An intermediate regime, 0.2–$0.8 \leqslant S/D \leqslant 2.4$–$2.8$, where the shear layers shed from the upstream cylinder reattach onto the downstream cylinder and shedding takes place behind the downstream cylinder. Also observed in this regime is the intermittent vortex formation behind the upstream cylinder.

(c) A regime of large spacing, $S/D \geqslant 2.8$, where vortices are shed from both cylinders.

The critical separation distance (2.5–4 cylinder diameters) for the onset of vortex shedding from both cylinders has been identified by many researchers (Xu & Zhou 2004; Zhou & Yiu 2005; Didier 2007; Liang *et al.* 2008; Mussa, Asinari & Luo 2009), both numerically and experimentally, for a wide range of Reynolds numbers, exhibiting a considerable variation with this parameter (Xu & Zhou 2004). The two-dimensional numerical simulations of Mittal *et al.* (1997), Meneghini *et al.* (2001) and Liang *et al.* (2008) showed a sharp increase of the drag coefficient and Strouhal number ($St = fD/U$, where f is the vortex shedding frequency), once this critical

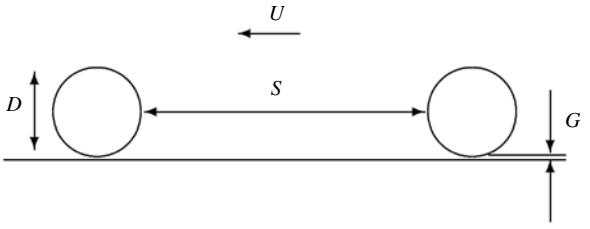

FIGURE 1. Schematic representation of the tandem cylinder problem, showing key parameters.

spacing was exceeded. This spacing has been commonly termed the drag inversion separation, where the drag coefficient of the downstream cylinder changes from negative to positive as the separation distance is increased.

The onset of unsteady flow was found to be delayed to higher Reynolds numbers at close separations. Mizushimaa & Suehiro (2005) concluded that the flow behind the upstream body is greatly stabilized by the presence of the downstream body and the transition to unsteady flow for spacings of $S/D = 1$ and $S/D = 3$ occurred at $Re = 68$ and $Re = 78.5$, respectively. This is much higher than the critical value observed for an isolated single cylinder ($Re \simeq 47$). It was also shown that the transition was supercritical for a spacing of $S/D = 1$ and subcritical at $S/D = 3$. For larger separations, an increase in the force coefficients was observed.

Flows past multiple cylinders, both in the proximity of a wall and in free stream, have been investigated by several researchers, e.g. Kumar, Sjarma & Agrawal (2008), Liang *et al.* (2008), Harichandan & Roy (2010) and Sewatkar *et al.* (2012). Kumar *et al.* (2008) and Sewatkar *et al.* (2012) found interesting nonlinear interactions between the wakes of multiple inline square cylinders, depending on inter-cylinder separation, with a variety of possible asymptotic states.

Two- and three-dimensional numerical simulations were performed by Deng *et al.* (2006) for $Re \geqslant 220$ and different separation distances. In their two-dimensional simulations at $Re = 220$ for $S/D \leqslant 2.5$, vortex shedding does not take place between the two cylinders, while for $S/D \geqslant 3$, each cylinder produces a vortex wake. However, in their three-dimensional simulations, three-dimensionality was observed for $S/D \geqslant 2.5$, but not for smaller spacings. For the critical spacing of $S/D = 2.5$, the transition to three-dimensionality occurs at $Re = 250$. Similar computations have been performed by Papaioannou *et al.* (2005) for tandem cylinder cases. Their simulations show an increase in three-dimensionality of the wake as the critical spacing distance was approached. At close spacings, the primary vortices were unable to roll up and form strong vortex cores, which reduces the sensitivity to three-dimensional effects and thereby stabilizes the flow.

Stability analysis for a tightly packed cylinder array was performed by Kevlahan (2007) for cylinders spaced by $S/D = 1.5$, and for the array being in line with, or at an angle of 45° to, the flow. For the inline cylinders, periodic flow was detected beyond $Re = 119$ and three-dimensional flow set in at $Re \simeq 132$, with the formation of mode A type structures of spanwise wavelength $3D$. He further reports that the mode B type structures are absent in cylinder arrays, since the braid structures are suppressed by the tight packing. At $Re = 200$, the growth rates of the three-dimensional modes were higher for the angled array than for the inline array.

The onset of three-dimensional flow for inline tandem cylinders for $S/D = 4$ resembled that for an isolated cylinder in a free stream (Carmo *et al.* 2008). The onset of the mode A type instability was observed at $Re = 180$ and mode B at $Re = 272$. Recent numerical investigations by Carmo, Meneghini & Sherwin (2010) of the flow around inline tandem cylinders in a free stream, showed the existence of three new modes at various separation distances for $Re \geqslant 200$. For small separations, the onset of three-dimensionality occurs via a mode T1, whose spatiotemporal symmetry resembles that of the mode B instability of an isolated cylinder at higher Reynolds numbers. This mode has a spanwise wavelength of $\sim 2D$. Two other modes were observed when the cylinders were spaced in the range $0.8 \leqslant S/D \leqslant 1.5$. The physical mechanism of the mode T2 instability is believed to be centrifugal, while mode T3 has characteristics similar to those of mode A of the single-cylinder wake. Mode T2 has a spanwise wavelength of $\sim 3D$, while mode T3 has a wavelength of $\sim 4.6D$ at onset. At large separations, the mode A instability is followed by the mode B instability, akin to the case of an isolated cylinder in a free stream.

Flow features behind a single cylinder near a wall have been discussed by several researchers (Stewart *et al.* 2006; Huang & Sung 2007; Mahir 2009; Stewart *et al.* 2010*b*; Rao *et al.* 2011, 2012). Stewart *et al.* (2010*b*) found that, for a cylinder sliding near a wall, the transition to unsteady flow was delayed to higher Reynolds numbers ($Re \simeq 160$), compared with a cylinder in a free stream. They further observed that the onset of three-dimensionality occurred at much lower Reynolds numbers ($Re \simeq 70$) in the steady flow regime. Experimental investigations in a water channel with a moving floor confirmed the flow structures observed in the numerical studies.

Very few studies have considered the flow features of multiple bodies moving along a wall. Bhattacharyya & Dhinakaran (2008) conducted numerical simulations for a pair of tandem square cylinders in a linear shear flow at $G/D = 0.5$, where G is the distance between the cylinder and the wall. Below $Re = 125$, the shear layers separating from the two sides, are unable to interact and cause vortex shedding. At a spacing of $S/D \leqslant 2$, the two cylinders effectively behave as one body at $Re \leqslant 200$. For $2 < S/D < 3$, vortices are shed from the downstream cylinder only. Above this range, vortices are shed from both cylinders and at even larger separation distances, the shedding frequency recorded for both cylinders match that of a single cylinder under similar flow conditions. The height above the wall and the separation distance both influence the shear layer interaction responsible for the formation of vortices. Harichandan & Roy (2012) performed numerical investigations for circular cylinders in tandem close to a wall at Reynolds numbers $Re = 100$ and 200 for separation distances of $S/D = 1$ and 4. The bodies were placed at $0.5D$ and $1D$ above the stationary wall. They observed that the variation of the separation distance has a stronger influence on the flow stability than changes in the gap to the wall. Vortex shedding occurred when the gap heights and the separation distance were both large. Rao *et al.* (2011) investigated the flow structures behind two tandem cylinders near a wall for $Re \leqslant 200$ and determined the drag coefficient on the cylinders. The drag on the downstream cylinder was found to be positive, which is in contrast to that observed at small separations for tandem cylinders in a free stream. This was attributed to the higher pressure forces experienced by the cylinders in the vicinity of the wall.

The present numerical study attempts to quantify the complex wake interactions that occur in the wake of a pair of tandem cylinders in close proximity to a wall for a range of longitudinal separation distances. The initial motivation for this study was to examine and better understand bluff-body/fluid and body/body interactions in the neighbourhood of a wall, where it is clear that the fluid dynamics is quite

distinct from that for interacting bodies away from a wall. In turn, this represents a step towards an improved understanding of fluid/particle and particle/particle physics relevant to multiphase systems for mineral and chemical processing applications, and the micro-physics of sedimentation.

The remainder of this article is organized as follows. The problem under consideration and the numerical formulation are described in § 2, along with domain size and spatial resolution studies. This is followed by the results from the numerical simulations in § 3, where the steady and unsteady flow regimes are mapped. The onset of three-dimensional flow in these regimes is investigated in § 4. To further investigate the fully developed three-dimensional wakes, direct numerical simulations (DNS) are performed and the flow structures for various separations visualized in § 5. This is followed by conclusions in § 6.

2. Numerical methods

2.1. *Problem definition*

Figure 1 shows a schematic of the flow problem under consideration. We investigate the flow over two identical tandem cylinders of diameter D, separated in the streamwise direction by a distance S, sliding along a wall at constant speed U. A small gap of size G is maintained between the cylinders and the wall to prevent the high-order mesh elements (see below) from becoming degenerate directly underneath. The gap ratio G/D is held fixed at 0.005 for both cylinders, after verifying that the effect on the downstream flow is negligible, in line with previous studies for single cylinders and spheres (Zeng, Balachandar & Fischer 2005; Stewart *et al.* 2006, 2010*a*,*b*; Rao *et al.* 2011, 2012). Although the shedding frequency is insensitive to the gap height, the force coefficients display a weak logarithmic variation as the gap height is reduced. There is further discussion of these issues in Stewart *et al.* (2010*a*,*b*) for a single cylinder and a sphere, including an examination of the minor flow through the gap and the variation of the force coefficients for small gap ratios. The fluid is assumed to be Newtonian and incompressible. For computational convenience, we employ a uniformly translating frame of reference attached to the cylinders, with the origin at the centre of the first cylinder. In this frame, the cylinders appear stationary, with both the far fluid and the wall moving to the right at uniform speed U. In the following, all quantities are non-dimensionalized with the cylinder diameter D and the free stream velocity U. The parameter ranges investigated are $20 \leqslant Re \leqslant 200$ and longitudinal spacing $0.1 \leqslant S/D \leqslant 10$.

2.2. *Numerical scheme*

The numerical approach is based on a spectral-element formulation to discretize the unsteady incompressible Navier–Stokes equations in two dimensions. The domain consists of a collection of quadrilateral elements with a higher element density in regions of high-velocity gradients near the cylinders and in the wake regions. These quadrilateral (or macro) elements are further subdivided internally into $N \times N$ nodes. The nodes correspond to Gauss–Legendre–Lobatto quadrature points, and the velocity and pressure fields are represented by tensor products of Lagrangian polynomial interpolants of order $N - 1$ within elements. The resolution can be set at runtime by selecting the number of internal node points. The method exhibits exponential convergence as N is increased (Karniadakis & Sherwin 2005), consistent with global spectral methods.

The unsteady discretized Navier–Stokes equations are then solved using a three-step time-splitting method, following an approach outlined by Chorin (1968) and described in more detail in Thompson *et al.* (2006*a*), and also see Karniadakis, Israeli & Orszag (1991). The three substeps account for advection using a third-order Adams–Bashforth method, pressure, which enforces local mass conservation and diffusion using a theta-damped Crank–Nicholson method. Second-order time accuracy is achieved for the velocity field by using a higher-order boundary condition for the pressure, enforcing mass conservation at boundaries (Karniadakis *et al.* 1991). Further details on the numerical code can be found in various articles (Ryan *et al.* 2005; Thompson *et al.* 2006*a*; Leontini, Thompson & Hourigan 2007). It has been previously used to investigate (and validated for) related problems such as flows past cylinders in a free stream (Thompson *et al.* 1996, 2001, 2006*b*; Leontini *et al.* 2007) and around bodies near a wall (Stewart *et al.* 2006; Thompson, Leweke & Hourigan 2007; Stewart *et al.* 2010*b*; Rao *et al.* 2011).

2.3. *Linear stability analysis*

Linear stability analysis is used here to determine the stability of the flow with respect to spanwise perturbations. The numerical approach is similar to that employed by Barkley & Henderson (1996), Blackburn & Lopez (2003), Sheard, Thompson & Hourigan (2003), Leontini *et al.* (2007), Griffith *et al.* (2009) and others. The Navier–Stokes equations are used to derive linearized equations for the velocity and pressure perturbation fields about a two-dimensional base flow, which are explicitly dependent on the spanwise coordinate. Because of the linearity and lack of spanwise dependence of the base flow, the spanwise dependence of the perturbation fields can be represented as a combination of Fourier modes, each of which can grow or decay exponentially in time. In practice, to determine stability, the linearized Navier–Stokes equations for the perturbation fields are marched forward in time until the fastest-growing or slowest-decaying Fourier mode dominates the solution. Alternatively, a Krylov subspace method can be used with Arnoldi decomposition to extract more of the most dominant modes (see, e.g., Mamun & Tuckerman 1995). The evolution (exponential growth or decay) of a given perturbation mode depends on its spanwise wavelength λ and the Reynolds number. The (linear) growth rate σ can be evaluated from the amplitude ratio at two instants in time, separated by a time interval T: $|A(t = t_0 + T)|/|A(t = t_0)| = \exp(\sigma T) = \mu$. For $\sigma > 0$ (or $|\mu| > 1$), the perturbations grow and three-dimensionality develops, while for $\sigma < 0$ (or $|\mu| < 1$), the perturbations die out. Neutral stability occurs for $\sigma = 0$ or $|\mu| = 1$. For periodic base flows, the time period for monitoring the growth is set to the base flow period, a process known as Floquet analysis, with μ being the Floquet multiplier. For flow past a single cylinder near a wall, three-dimensional flow usually occurs in the steady flow regime, prior to the onset of periodic flow (Stewart *et al.* 2010*b*; Rao *et al.* 2011). For periodic flows, the three-dimensional modes may also have a periodicity different to the oscillatory base flow, in which case the Floquet multipliers are complex (Blackburn & Lopez 2003; Elston, Blackburn & Sheridan 2006; Leontini *et al.* 2007). Such methods have been used previously to resolve subharmonic modes in the wake behind rings (Sheard *et al.* 2003; Sheard, Thompson & Hourigan 2005) and inclined square cylinders (Sheard, Fitzgerald & Ryan 2009; Sheard 2011). More details on this method and its implementation can be found in Leontini *et al.* (2007), Stewart *et al.* (2010*b*) and Rao *et al.* (2011).

	$Re = 20$		$Re = 200$		$Re = 200$	
N^2	$\overline{C}_{dD}$	% variation	$\overline{C}_{dD}$	% variation	St	% variation
5^2	10.097389	0.1398206	1.732380	−2.035431	0.090208	−0.898475
6^2	10.102081	0.0934181	1.708033	−0.601417	0.089602	−0.220676
7^2	10.110580	0.0093655	1.704390	−0.386848	0.089509	−0.116657
8^2	10.111458	0.0006824	1.700441	−0.154256	0.089451	−0.051785
9^2	10.111456	0.0007021	1.699990	−0.127693	0.089447	−0.047311
10^2	10.111518	0.0000890	1.698354	−0.031334	0.089417	−0.013757
11^2	10.111527	0	1.697822	0	0.089407	0

TABLE 1. Variation of the time-averaged drag coefficient of the downstream cylinder ($\overline{C}_{dD}$) and shedding frequency (St) for $S/D = 10$ at the specified Reynolds numbers (Re).

2.4. *Effect of domain size*

The domain is defined in terms of the location of the inlet, top and outlet boundaries relative to the cylinders. Several meshes were constructed with their boundaries placed at different distances from the cylinders. For these investigations, the simulations were run at $Re = 200$ with a polynomial order of $N = 7$ for the cylinders separated by the maximum distance considered of $S/D = 10$. The inlet and the lateral/top boundaries were placed between $25D$ and $100D$ from the leading cylinder, and the outlet boundary between $50D$ and $200D$ downstream of the trailing cylinder. The simulations were run for the same time interval and the forces on the cylinders were monitored. The time-averaged drag coefficient of the downstream cylinder was computed from the force histories. Periodic flow was observed for this case and the Strouhal number was also computed. Based on the results, the values $50D$, $100D$ and $50D$ were chosen for the inlet and outlet distances and the domain height, respectively. With this choice, the mean drag coefficient and the Strouhal number differed by less than 0.5 and 0.6 %, respectively, from the values obtained with the largest domain.

2.5. *Effect of mesh resolution*

The number of macroelements varies with the separation distance and is significantly higher than that required for previous single cylinder studies. One advantage of the spectral-element method is the ability to specify the number N of internal node points on each edge, and therefore the resolution, at runtime. Once a reasonable macroelement distribution is established, the resolution can then be further controlled by varying N. The maximum separation distance ($S/D = 10$) was chosen in order to test the value of N required to resolve the flow correctly. The number of node points in each macroelement was varied between $N^2 = 5^2$ and $N^2 = 11^2$, and tests were performed at two Reynolds numbers of 20 and 200. The resolution of $N^2 = 4^2$ was insufficient to capture the flow characteristics, while $N^2 = 12^2$ proved to be computationally expensive with a strong (Courant) restriction on the time step. The simulations for the grid resolution study used a fixed non-dimensional time step of $\Delta\tau = 0.001$. Table 1 shows the variation of the time-averaged drag coefficient of the downstream cylinder, $\overline{C}_{dD}$, and the Strouhal number, as the resolution is varied. For $N^2 = 7^2$, the variation in $\overline{C}_{dD}$ and St is less than 0.5 and 0.15 %, respectively, relative to the most resolved case. Computations at $Re = 20$ showed a variation of

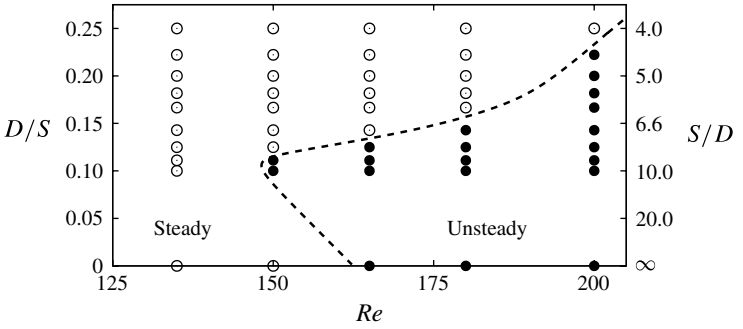

FIGURE 2. Transition diagram showing the onset of unsteady state with Reynolds number (Re) for $0 \leqslant D/S \leqslant 0.25$. The steady flow regime is marked by open symbols (○) and the unsteady flow regime is marked by closed symbols (●). Steady flow was observed for all spacings at $Re = 135$. The dashed line shows the approximate demarcation between the steady and unsteady flow regimes.

less than 0.1 % at $N^2 = 7^2$ compared with the highest resolution tested. Thus an inter-element resolution of $N^2 = 7^2$ was chosen for all computations, since it provided an acceptable accuracy for a reasonable computational effort.

3. Two-dimensional flow

3.1. *Flow structures*

The flow past a single cylinder sliding along a wall was investigated by Stewart *et al.* (2006, 2010*b*). Two recirculation zones form in the near wake of the cylinder, whose lengths vary linearly with Reynolds number. The recirculation zones extend to a maximum of approximately $8D$ downstream of the cylinder at $Re = 150$, above which unsteady periodic flow occurs. The shear layer moving over the cylinder and the induced wall boundary layer form vortex pairs, which drift downstream of the cylinder. The flow features associated with two tandem cylinders *rolling* along a wall were previously investigated by Rao *et al.* (2011). At large separation distances, unsteady flow was encountered at high Reynolds numbers, while steady flow was found at low Reynolds numbers. In a similar way, we here investigate the onset of periodic flow for *sliding* tandem cylinders, in the range of spacings $4 \leqslant S/D \leqslant 10$ for $Re \leqslant 200$.

Figure 2 presents the transition map, showing the onset of unsteady flow as the Reynolds number and cylinder spacing are varied. In this plot, the inverse of the separation distance, D/S, is used, in order to include the isolated cylinder case ($D/S = 0$). Unsteady flow is observed at $Re = 150$ for cylinders with $S/D = 9$ and 10. This is slightly below the critical Reynolds number for the transition to the unsteady regime for an isolated cylinder sliding along a wall ($Re_c \simeq 160$) (Stewart *et al.* 2010*b*). At higher Reynolds numbers, unsteady flow occurs at smaller spacings, as predicted by Rao *et al.* (2011). At the maximum Reynolds number tested, $Re = 200$, unsteady flow was observed at a separation distance as low as $S/D = 4.5$.

As mentioned above, the steady wake of a single cylinder near a wall comprises two recirculation zones. For two cylinders at very close spacings, a similar wake structure is found behind the downstream cylinder. As the spacing is increased, multiple recirculation zones are observed in the gap between the cylinders (figure 3), which remain steady even at higher Reynolds numbers. These zones are similar to

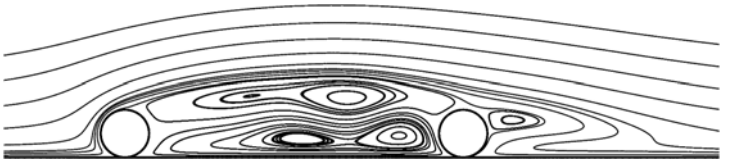

FIGURE 3. Streamlines of the flow past tandem cylinders for $S/D = 6$ at $Re = 180$. Multiple recirculation zones are observed in the space between the cylinders. The cylinders are translating from right to left.

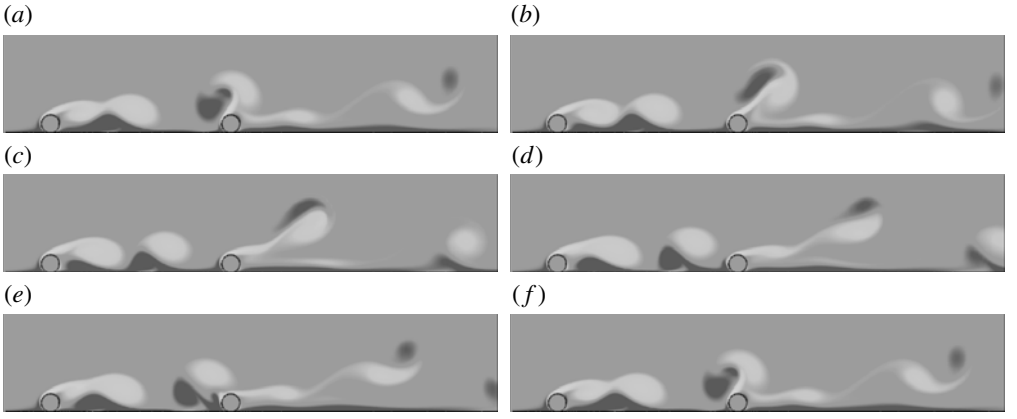

FIGURE 4. Instantaneous vorticity fields at $Re = 200$, for $S/D = 9$. Time t is expressed in terms of the shedding period T: (*a*) $t = 0$; (*b*) $t = T/5$; (*c*) $t = 2T/5$; (*d*) $t = 3T/5$; (*e*) $t = 4T/5$; (*f*) $t = T$. The cylinders are translating from right to left, and vorticity contours cover the range $\pm 5U/D$.

what Igarashi (1981) described as quasi-stationary vortices, which occur in the range $1 \leqslant S/D \leqslant 2.5$ for cylinders in a free stream, prior to the onset of unsteady flow.

The process of vortex shedding, found in the unsteady periodic regime, is illustrated in figure 3, showing a sequence of vorticity distributions in the near wake during one shedding cycle for $S/D = 9$ and $Re = 200$. In the first snapshot, the separating shear layer from the top of the upstream cylinder is beginning to roll up. The presence of this primary vorticity induces secondary vorticity at the wall underneath it. This secondary vorticity is pulled away from the wall between two successive primary vortex structures. In later images, the previously shed primary vortex and the rolled-up secondary vorticity combine into a non-symmetrical vortex pair, which impinges on the downstream cylinder and subsequently moves away from that cylinder at an oblique angle due to self-induction. Since the primary vorticity is stronger, and because it is also supplemented by more vorticity separating from the second cylinder, the combined structure moves closer to the wall as it travels downstream. At $\sim 10D$ downstream of the second cylinder, the remaining clockwise vorticity again induces secondary vorticity at the wall, which is pulled away from the wall to combine with the primary vorticity to form a new vortex pair. This reformed pair then moves away from the wall through self-induction as the structure advects further downstream (not shown).

	$Re = 150$	$Re = 165$	$Re = 180$		$Re = 200$	
S/D	St_1	St_1	St_1	St_2	St_1	St_2
4.5	—	—	—	—	0.0887	—
5	—	—	—	—	0.0871	—
5.5	—	—	—	—	0.0880	—
6	—	—	—	—	0.0884	—
7	—	—	0.0895	0.0447	0.0461	0.0922
8	—	0.0889	0.0879	—	0.0875	0.0437
9	0.0892	0.0877	0.0878	—	0.0878	—
10	0.0877	0.0872	0.0888	—	0.0893	—
∞	—	0.1004	0.0982	—	0.0983	—

TABLE 2. Variation of St with S/D at the specified Re. The data for $S/D = \infty$ is taken from Stewart *et al.* (2010*b*).

3.2. *Strouhal numbers*

The drag coefficient was monitored for several hundred units of non-dimensional time τ ($=tU/D$), in order to compute the shedding frequency. Table 2 shows the variation of the Strouhal number with separation distance for the parameter range studied, along with the results of Stewart *et al.* (2010*b*), where an isolated cylinder near a wall was investigated at similar Reynolds numbers. Their case is denoted by $S/D = \infty$, implying that the trailing cylinder is at a very large distance. The transition diagram (figure 2) shows that for $S/D \simeq 10$ the flow becomes unsteady at Reynolds numbers lower than the limit for an isolated cylinder near a wall. Presumably this can be attributed to the complex flow upstream of the second cylinder due to the presence of the first cylinder (figure 3). Shedding is synchronous from both cylinders, and a single frequency is detected from the Fourier spectra of the drag histories. At $Re = 150$ and 165, a slight decrease in St is observed as the spacing is increased.

The time histories of the drag coefficient for the downstream cylinder at $Re = 200$, for the separation distances in the range $6 \leqslant S/D \leqslant 9$ are shown in figure 5. The frequency spectra in figure 6 were obtained from the time history of the drag coefficient of the upstream cylinder over a period of approximately 50 shedding cycles. At $S/D = 7$ and 8, the waveform of the drag history clearly indicates the presence of two dominant frequencies, which were found to be integer multiples of each other. For $S/D = 7$, the dominant Strouhal number St_1 in terms of power spectral density (see table 2) is one half of the second strongest frequency St_2, while at a slightly larger spacing of $S/D = 8$, the value of the dominant Strouhal number is twice St_2. For both of these cases there are other frequency peaks in the power spectra corresponding to harmonics of the lowest frequency. At $Re = 180$, the drag history for $S/D = 7$ also contains two frequencies, while for spacings below or above this value only a single strong frequency component is observed.

The reason for the commensuration of frequencies can be seen by visualizing the wake for different separation distances using vorticity contours. Shown in figure 7 is the sequence of images over one cycle of shedding for $S/D = 6$, where a single peak is observed in the frequency spectrum. We observe that the shear layer (light grey) separating from the upstream cylinder rolls up into a vortex which generates and lifts up a wall boundary layer (dark grey) before striking the downstream cylinder. The rolled-up shear layer convects further downstream, where it draws more opposite-

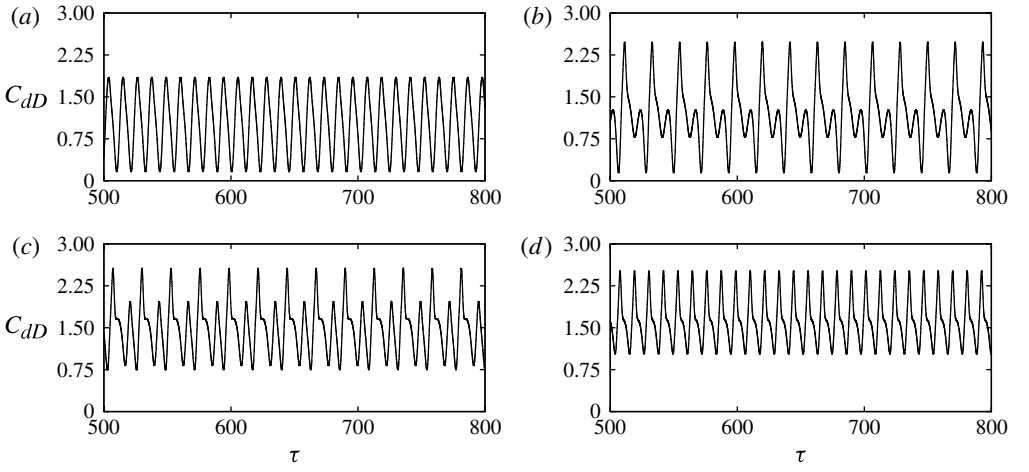

FIGURE 5. Time histories of the drag coefficient for the downstream cylinder (C_{dD}) at $Re = 200$ for the specified separation distances: (*a*) $S/D = 6$; (*b*) $S/D = 7$; (*c*) $S/D = 8$; (*d*) $S/D = 9$.

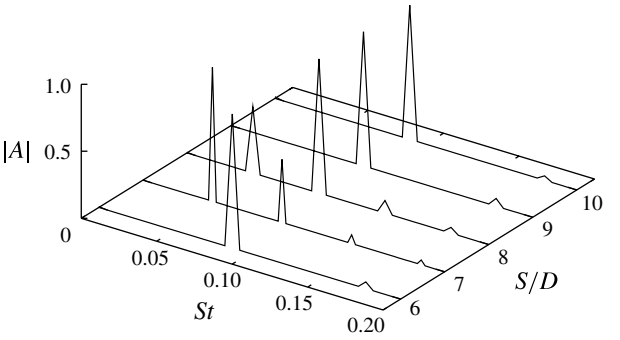

FIGURE 6. Fourier spectra for different spacings at $Re = 200$. Multiple peaks are found for $S/D = 7$ and $S/D = 8$. See the text for details.

signed boundary layer vorticity from the wall to form a vortex pair, which then advects away from the wall through self-induction. At a slightly larger separation distance of $S/D = 7$, stronger and weaker vortex structures are formed alternately from the shear layer separating from the first cylinder. This behaviour is clearly evident in the sequence of images in figure 8. Comparing figure 8(*c,h*), the structure of the separated shear layer between the cylinders is distinctly different. In the first case, the second rolled-up clockwise vortex structure of the shear layer is considerably stronger. The vortex draws the secondary vorticity from the boundary to form a vortex pair, which collides with the second cylinder before moving obliquely away from it. In the second case, the clockwise vorticity is weaker and does not draw boundary layer vorticity into the main flow. The clockwise vorticity merges smoothly with the shear layer separating from the second cylinder. The result is a very different behaviour between the two halves of the cycle. The period of shedding is approximately twice that observed for $S/D = 6$. This phenomenon is similar to the lock-in phenomenon

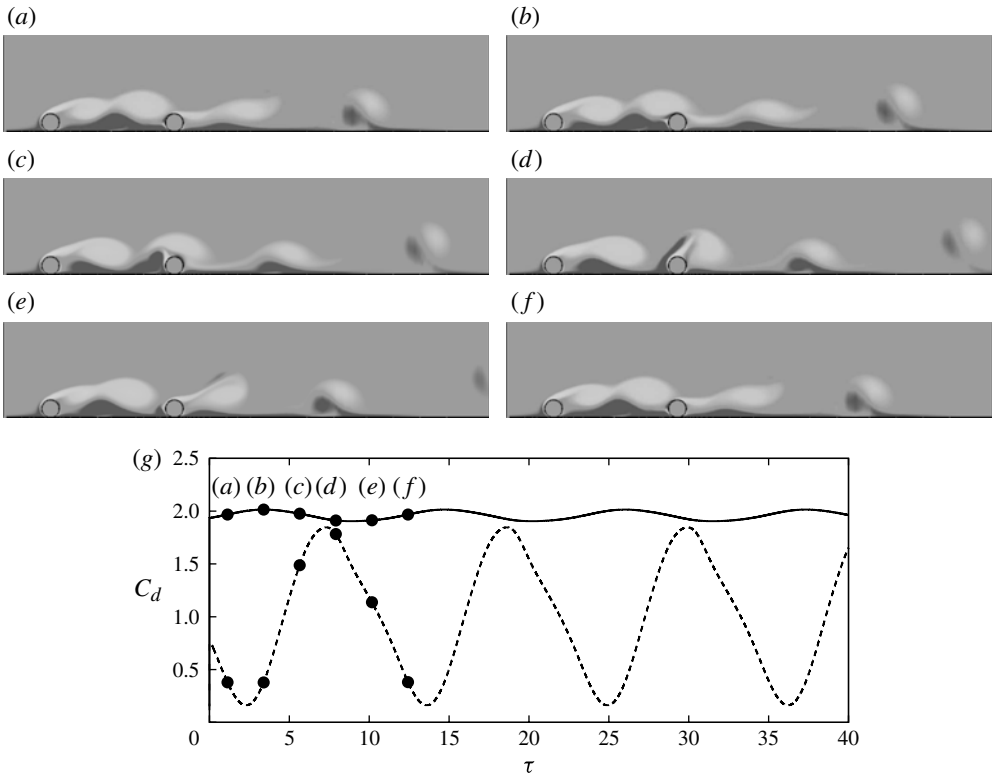

FIGURE 7. (*a–f*) Instantaneous vorticity contours at $Re = 200$ for $S/D = 6$. (*g*) Drag histories for the upstream (solid line) and downstream (dashed line) cylinders, showing the times corresponding to (*a–f*): (*a*) $t = 0$; (*b*) $t = T/5$; (*c*) $t = 2T/5$; (*d*) $t = 3T/5$; (*e*) $t = 4T/5$; (*f*) $t = T$.

observed in the wakes of elongated bluff bodies, where the timing of leading-edge vortices passing the trailing edge (equivalent to the second cylinder in the present configuration) controls the roll-up and shedding of further leading-edge vortices (Hourigan, Thompson & Tan 2001). For $S/D = 8$, the behaviour is similar to that for $S/D = 7$, while for $S/D = 9$ (see figure 3), the system period corresponds again to a single shedding cycle of the leading cylinder (rather than two leading-cylinder shedding cycles as for $S/D = 7$ or 8). A similar phenomenon is observed in the flow past six inline square cylinders (Sewatkar *et al.* 2012), where the flow transitions from a synchronous mode to a quasi-periodic mode and finally to a chaotic flow state.

3.3. *Drag trends*

The forces experienced by the cylinders were quantified by the direct summation of the pressure and viscous forces on the cylinders. The variation of the drag coefficient for the upstream and downstream cylinders is shown in figure 9 at different Reynolds numbers. The drag on the downstream cylinder was found to be much lower than that on the upstream cylinder for close spacings, as the upstream cylinder experiences a considerably larger pressure force than the downstream cylinder. However, at all spacings investigated here, the drag on both cylinders is positive. This can be attributed to the cylinders being close to the wall, where a higher pressure force

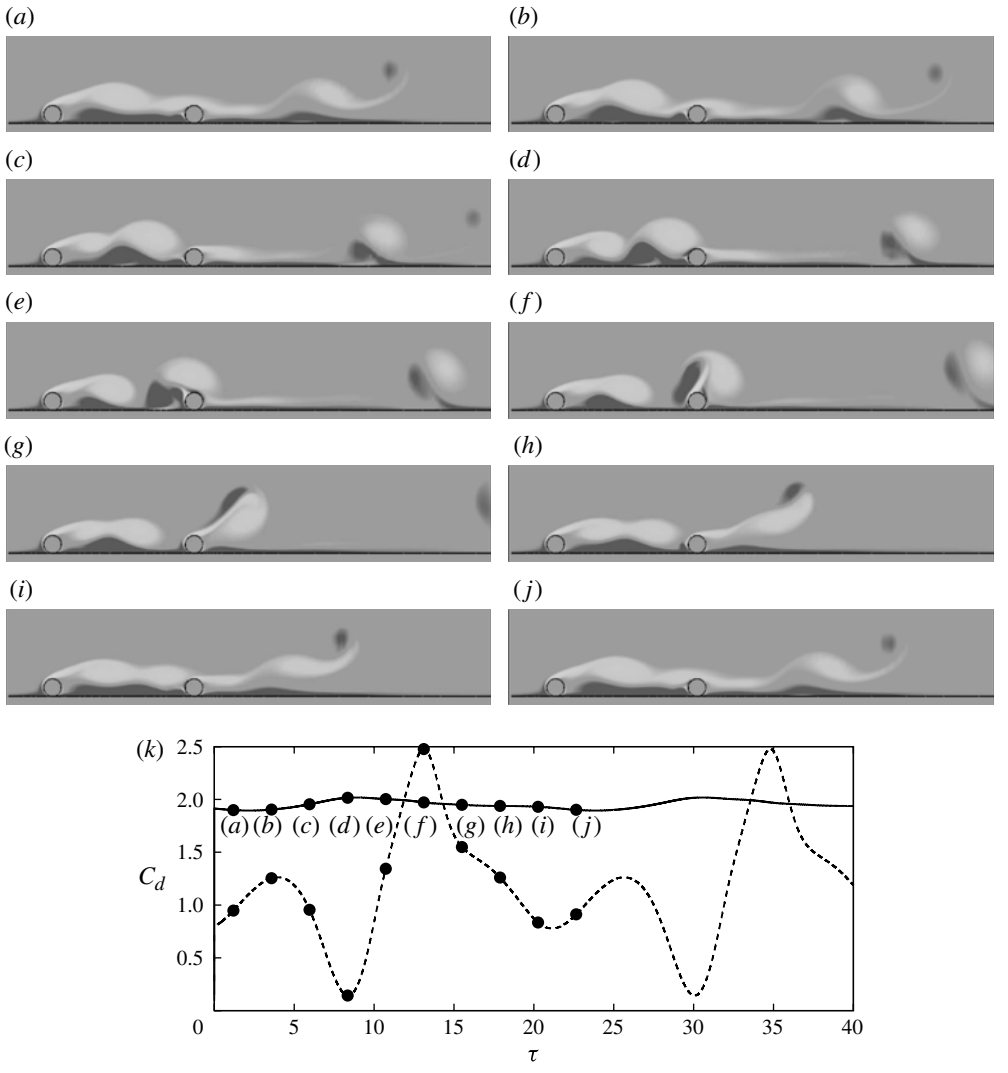

FIGURE 8. Same as figure 7 for $S/D = 7$. The period T of the flow oscillations is now twice the shedding period of the leading cylinder: (*a*) $t = 0$; (*b*) $t = T/9$; (*c*) $t = 2T/9$; (*d*) $t = 3T/9$; (*e*) $t = 4T/9$; (*f*) $t = 5T/9$; (*g*) $t = 6T/9$; (*h*) $t = 7T/9$; (*i*) $t = 8T/9$; (*j*) $t = T$.

acts on the upstream face of each cylinder. As expected, the drag coefficient on the downstream cylinder increases, as the spacing between the cylinders grows. When the cylinders are placed further apart, they behave increasingly as individual bodies. At higher Reynolds numbers, the flow is unsteady, and higher mean drag is experienced by the downstream cylinder. At $Re = 200$, the drag coefficient on the downstream cylinder approaches that experienced by the upstream cylinder. The vertical error bars indicate one standard deviation from the mean value for the unsteady flow cases.

Shown in figure 10 are phase plots for the drag coefficients of the upstream and downstream cylinders in the unsteady regime for the specified separation distances. They show the complex phase relationships between the forces acting on the two

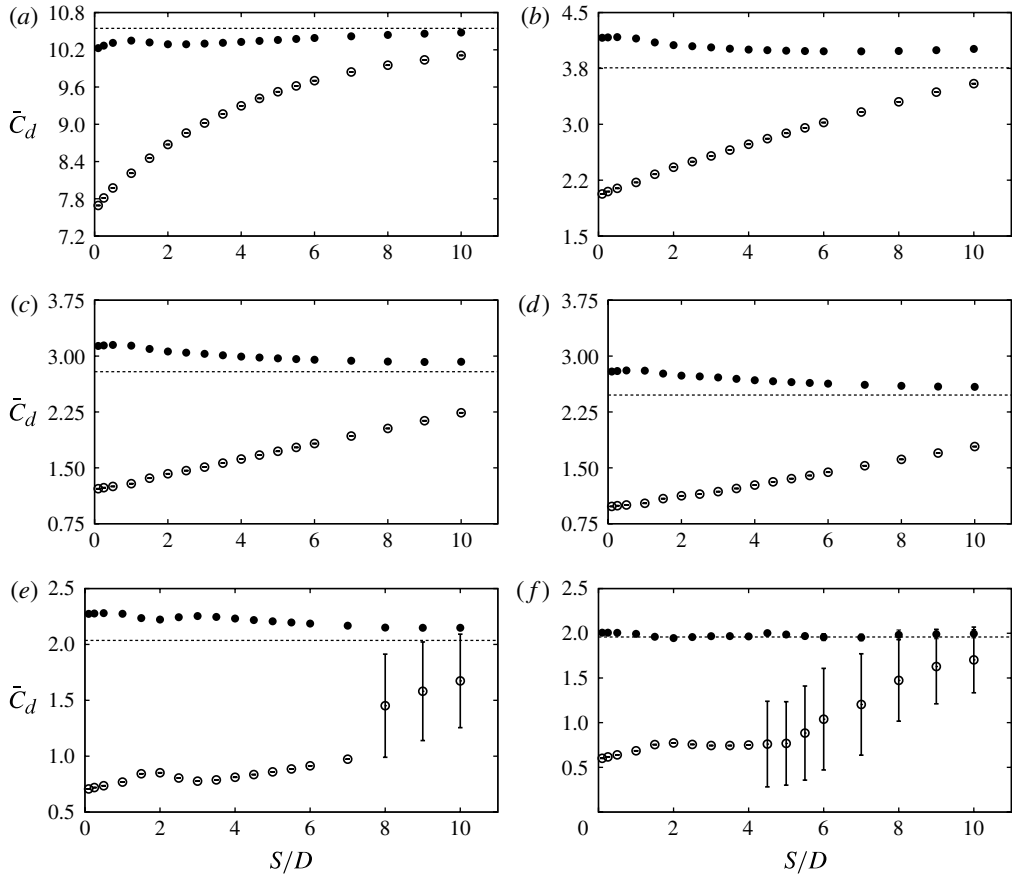

FIGURE 9. Drag trends at the specified Reynolds numbers. The filled circles (•) and the open circles (○) indicate the time-averaged drag coefficient on the upstream and downstream cylinders, respectively. In the unsteady regime, vertical error bars are used to represent one standard deviation of the instantaneous force coefficients. The time-averaged drag coefficient for an isolated cylinder at the corresponding Reynolds number is shown by a dashed line: (*a*) $Re = 20$; (*b*) $Re = 65$; (*c*) $Re = 100$; (*d*) $Re = 120$; (*e*) $Re = 165$; (*f*) $Re = 200$.

cylinders, in particular for the cases discussed above, where two dominant frequencies are present in the drag histories.

4. Three-dimensional stability

In this section, we investigate the stability of the two-dimensional base flow obtained in the previous section with respect to three-dimensional perturbations. Linear stability analysis is initially performed for the steady-state regime to detect the initial three-dimensional modes that grow at low Reynolds number. We employ the Arnoldi method based on a Krylov subspace to obtain the growth rate of the first few dominant modes, which can be either real or complex. For a single cylinder sliding along a wall, the flow undergoes a transition to three-dimensionality, with a spanwise wavelength $\lambda/D = 5.5$, at $Re = 71$ (Stewart *et al.* 2010*b*), which is below the threshold for the transition to unsteadiness of the two-dimensional flow at $Re = 160$.

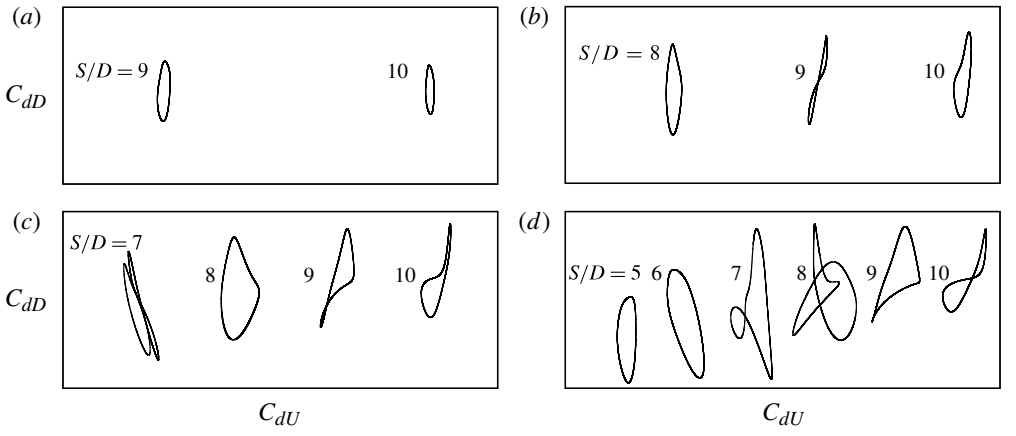

FIGURE 10. Phase plots showing the variation of the drag coefficient of the upstream (C_{dU}) and downstream (C_{dD}) cylinders at the specified Reynolds numbers: (*a*) $Re = 150$; (*b*) $Re = 165$; (*c*) $Re = 180$; (*d*) $Re = 200$.

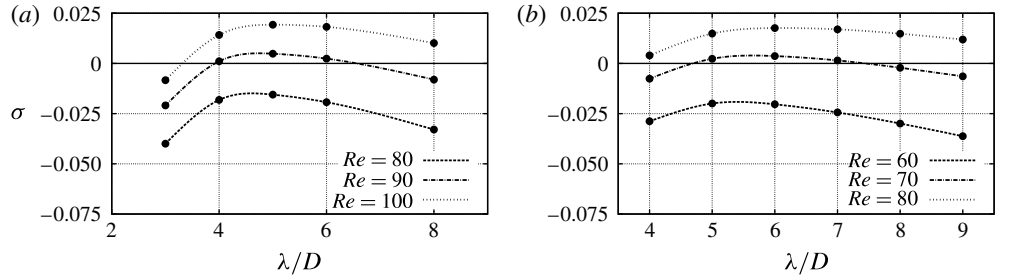

FIGURE 11. Growth rate curves for (*a*) small and (*b*) large spacing, about the critical Reynolds numbers for three-dimensional transition: (*a*) $S/D = 0.1$; (*b*) $S/D = 10$.

4.1. *Steady base flow*

Simulations were performed in the steady flow regime for the entire range of separation distances investigated previously. Examples of growth rate curves are given in figure 11 for a small and a large spacing between cylinders. Growth rates (σ) are shown as function of the perturbation wavelength for different Reynolds numbers, illustrating how the corresponding modes shift from stable ($\sigma < 0$) to unstable ($\sigma > 0$) as Re is increased.

Figure 12 shows the perturbation vorticity contours for different separation distances. The images shown are at Reynolds numbers just beyond the onset of three-dimensional flow. For small S/D, large amplitudes occur downstream of the trailing cylinder, while in the gap region the amplitude is small. When the separation distance between the two cylinders is large, the maximum mode amplitudes occur inside the gap. The perturbation field resembles that of an isolated sliding cylinder near a wall (Stewart *et al.* 2010*b*). The Floquet multiplier for the cases shown is real and positive.

Figure 13 shows the variation with separation distance of the critical Reynolds numbers for the three-dimensional transition and the corresponding instability wavelength. The critical values were obtained by polynomial interpolation from the

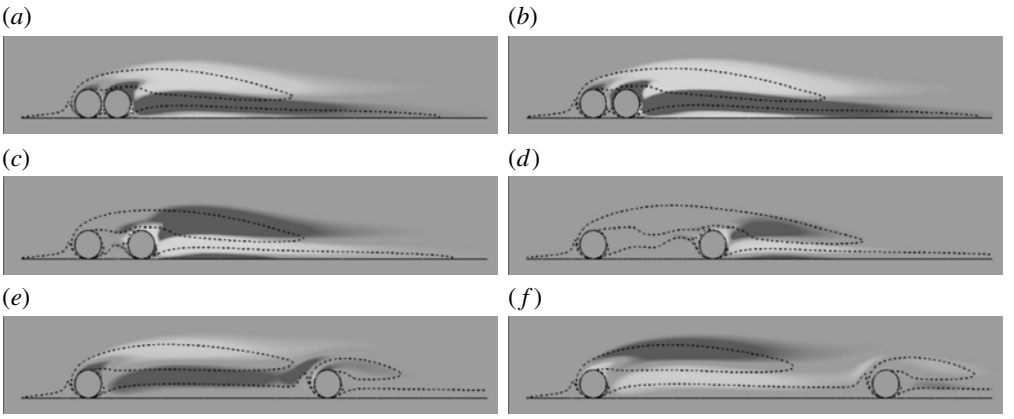

FIGURE 12. Spanwise perturbation vorticity contours for different separation distances at the specified Reynolds numbers and wavelengths. Perturbation vorticity contours are chosen to highlight the spatial distribution of the perturbation fields and base flow vorticity contour levels $\pm 1D/U$ are overlaid as dotted lines: (*a*) $S/D = 0.1$, $Re = 100$, $\lambda/D = 5$; (*b*) $S/D = 0.25$, $Re = 100$, $\lambda/D = 5$; (*c*) $S/D = 1$, $Re = 110$, $\lambda/D = 4$; (*d*) $S/D = 3.5$, $Re = 150$, $\lambda/D = 4$; (*e*) $S/D = 8$, $Re = 80$, $\lambda/D = 6$; (*f*) $S/D = 10$, $Re = 80$, $\lambda/D = 6$.

growth rate curves at Reynolds numbers above and below the critical values. For large spacings ($S/D \geqslant 7$), these values are quite close to those observed for a single sliding cylinder.

The transition to three-dimensionality for intermediate spacings occurs in a more complex way. For $4.5 \leqslant S/D \leqslant 6.5$, an initial transition to three-dimensionality occurs at low Reynolds number, followed by a re-stabilization of the flow to a two-dimensional state as the Reynolds number is increased (dotted line in figure 13). Increasing the Reynolds number further, the flow once again undergoes a transition to a new three-dimensional state, involving either a steady or an unsteady mode (see below).

This surprising sequence of stable two-dimensional and unstable three-dimensional regimes is further illustrated in figure 14, where growth rate curves for the case with $S/D = 5$ are shown. In figure 14(*a*), the growth rates for $Re < 100$ illustrate the first three-dimensional transition at $Re = 69.5$. Increasing the Reynolds number to 110, the maximum growth rates decrease, and at $Re = 120$ the flow is found to be stable (i.e. two-dimensional) again (figure 14*b*). Further increasing Re, a second transition to three-dimensional flow is found at $Re \simeq 157$ for a significantly smaller wavelength of $\lambda/D = 3.4$ (figure 14*c*), i.e. involving a different instability mode. Spanwise perturbation vorticity is plotted for $S/D = 5$ in figure 15 for both three-dimensional transitions. For the first transition, three-dimensionality develops in the space between the two cylinders, while for the second one, the growth of perturbations occurs downstream of the trailing cylinder.

For comparison, the case with $S/D = 6$, which also exhibits two successive three-dimensional transitions, is illustrated in figure 16. In this case, both modes have high amplitudes within the gap region between the cylinders, although the perturbation vorticity patterns are quite distinct. However, the growth rate for the second transition has a non-zero imaginary part, indicating that the flow is periodic, while for the first transition the growth rate is purely real.

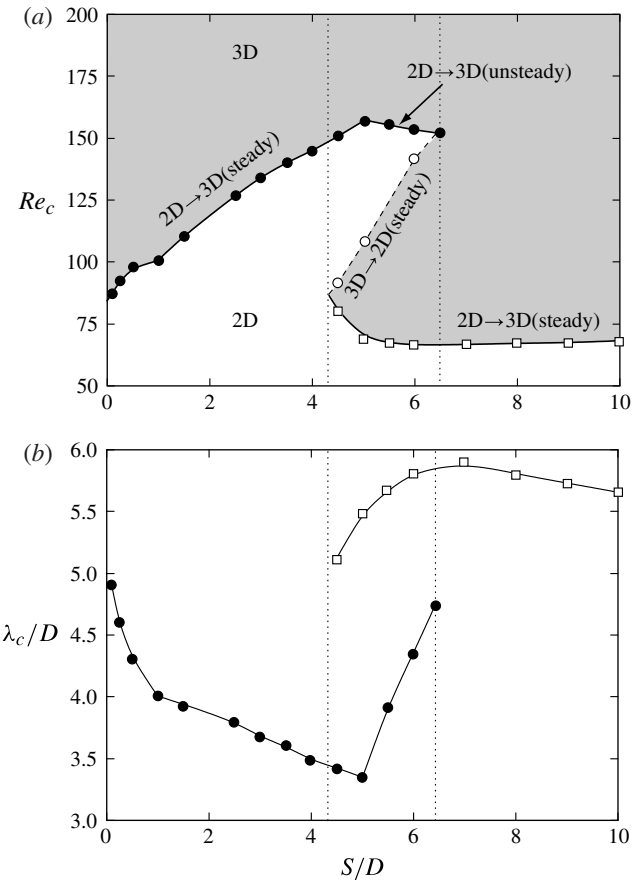

FIGURE 13. Variation with S/D of (a) the critical Reynolds number(s) and (b) the critical wavelength(s) for three-dimensional transition. Data concerning the same transition are represented by identical symbols.

As mentioned above, the two-stage instability scenario occurs for spacings in the range $4.5 \leqslant S/D \leqslant 6.5$. A further investigation was undertaken by carrying out stability analysis at higher Reynolds numbers for separation distances on either side of this range. The spanwise perturbation vorticity contours corresponding to the two smaller separation distances of $S/D = 0.25$ and 3 are shown in figure 17. Comparing figures 17(a) and 12(b), we observe that the three-dimensional modes possess identical structure, although at $Re = 180$ the length of the recirculation zone is longer than at $Re = 100$. The perturbation fields are broadly similar to the single cylinder case, so that the two cylinders are effectively acting as a single extended body.

In figure 18, streamwise perturbation vorticity contours are shown for almost touching cylinders ($S/D = 0.1$) at $Re = 150$. The structure of the perturbation contours bears a close resemblance to that of figure 22(b) in Stewart *et al.* (2010*b*), although the Reynolds number in this case is much higher, indicating that the three-dimensional modes involved are effectively identical.

The perturbation modes for higher S/D are depicted in figure 20. Their shape is clearly different from the mode structure for smaller separations. The strong

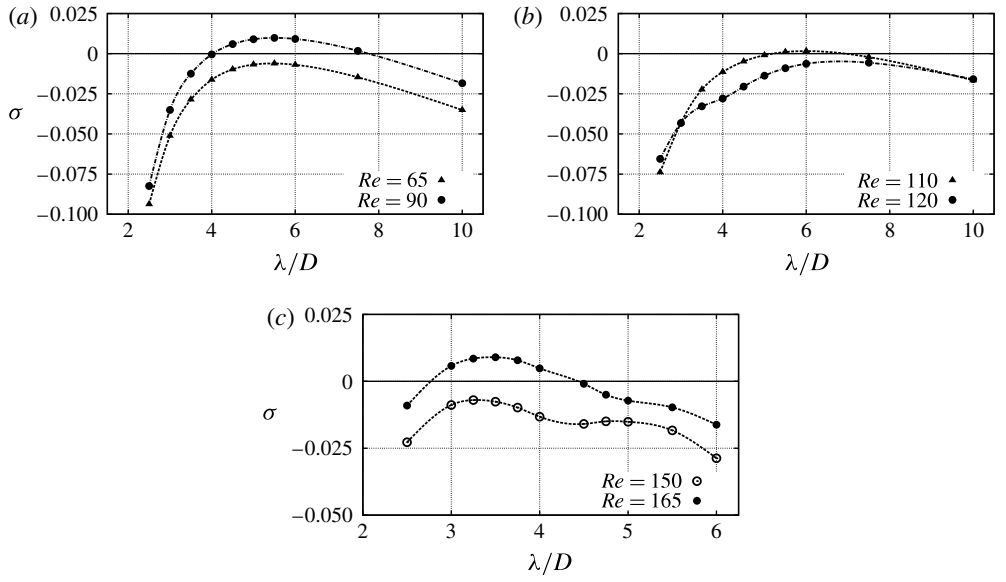

FIGURE 14. Growth rate curves for $S/D = 5$. (*a*) and $Re < 100$. The initial transition occurs at $Re \simeq 70$. (*b*) $Re > 100$. The flow returns to a two-dimensional state at $Re \simeq 120$. (*c*) $Re \geqslant 150$. A second transition to three-dimensionality occurs at $Re \simeq 157$.

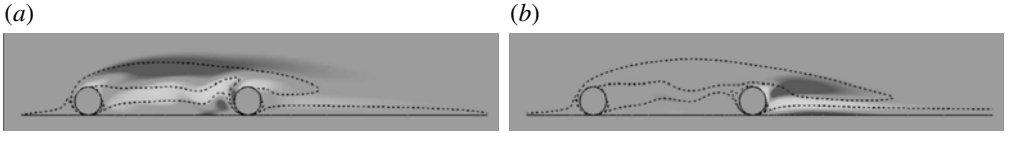

FIGURE 15. Spanwise perturbation vorticity for (*a*) the first and (*b*) the second transition to three-dimensionality for $S/D = 5$. Contour shading as in figure 12: (*a*) $Re = 75$, $\lambda/D = 5.5$; (*b*) $Re = 165$, $\lambda/D = 3.5$.

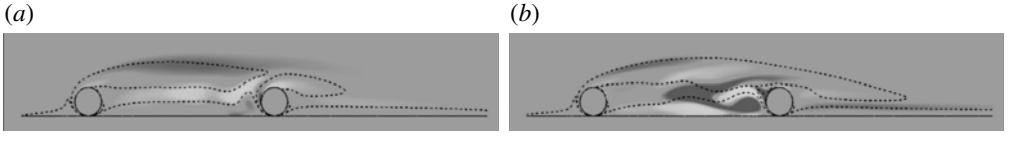

FIGURE 16. Spanwise perturbation vorticity for (*a*) the first and (*b*) the second transition to three-dimensionality for $S/D = 6$. Contour shading as in figure 12: (*a*) $Re = 80$, $\lambda/D = 6$; (*b*) $Re = 165$, $\lambda/D = 5$.

flow within the gap and the significant streamline curvature, with strong localized recirculations towards the second cylinder, modifies the unstable three-dimensional mode shape (figure 20*a,b*). This effect is less pronounced at larger separations, where once again the perturbation field tends towards the one for a single cylinder (figure 20*c,d*).

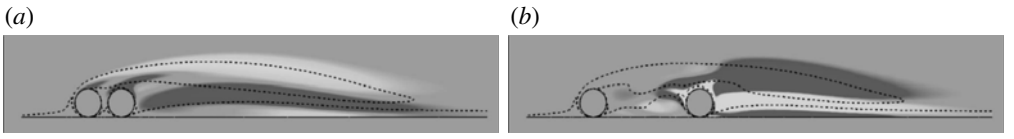

FIGURE 17. Spanwise perturbation vorticity contours for lower S/D. Contour shading as in figure 12: (*a*) $S/D = 0.25$, $Re = 180$, $\lambda/D = 10$; (*b*) $S/D = 3$, $Re = 180$, $\lambda/D = 5$.

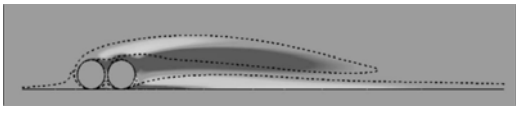

FIGURE 18. Streamwise perturbation vorticity contours for $S/D = 0.1$ at $Re = 150$, with $\lambda/D = 8$. Contour shading as in figure 12.

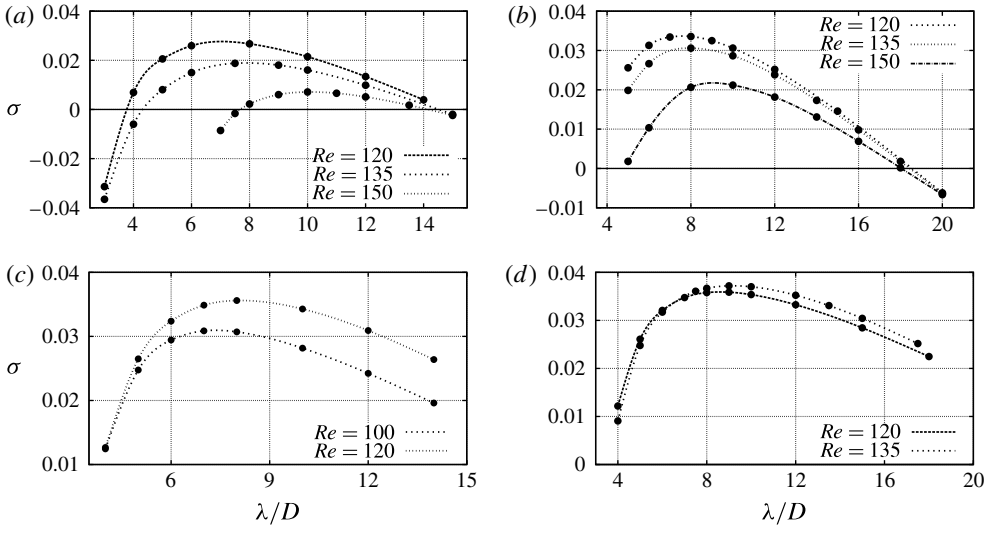

FIGURE 19. Growth rate curves at higher Reynolds numbers for higher S/D: (*a*) $S/D = 7$; (*b*) $S/D = 8$; (*c*) $S/D = 9$; (*d*) $S/D = 10$.

For the case with $S/D = 7$, $Re = 165$ represents the highest Reynolds number at which the two-dimensional flow remains steady. For this parameter combination, the flow was found to be unstable to two different three-dimensional modes. The growth rate of the longer-wavelength mode, as a function of Reynolds number, was given in figure 19(*a*). Figure 21 shows that this mode still remains unstable at $Re = 165$; however, a shorter-wavelength mode is now even more unstable. The maximum growth rates of these two modes occur at $\lambda/D \simeq 4.5$ and 12, respectively (figure 21). The short-wavelength mode is periodic, with a complex growth rate, while the long-wavelength mode is stationary (purely real growth rate). The perturbation vorticity contours of these two modes are shown in figure 22. However, the flow at this Reynolds number appears to be three-dimensional and unsteady with an associated

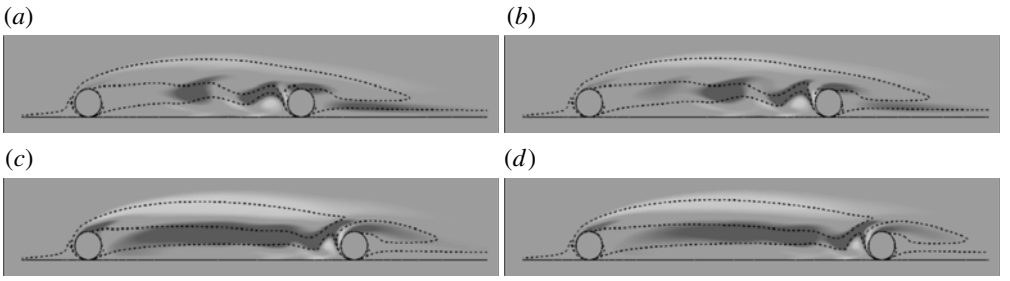

FIGURE 20. Spanwise perturbation vorticity contours for higher S/D. Contour shading as in figure 12: (*a*) $S/D = 7$, $Re = 150$, $\lambda/D = 10$; (*b*) $S/D = 8$, $Re = 150$, $\lambda/D = 10$; (*c*) $S/D = 9$, $Re = 120$, $\lambda/D = 8$; (*d*) $S/D = 10$, $Re = 135$, $\lambda/D = 9$.

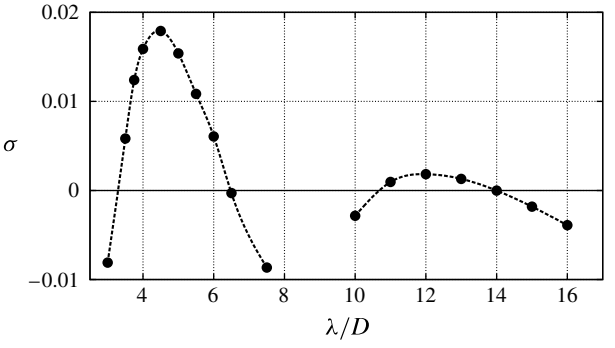

FIGURE 21. Growth rate curves for $S/D = 7$ at $Re = 165$. Two modes are present at this Reynolds number, including the one decaying as Re increases shown in figure 19(*a*).

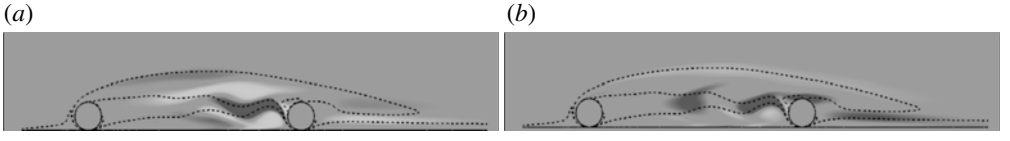

FIGURE 22. Spanwise perturbation vorticity contours for $S/D = 7$ at $Re = 165$ for the two instability modes at the specified wavelengths. The decaying mode is shown in (*b*). The perturbation contours of this mode are similar to that observed in figure 20(*a*). Contour shading as in figure 12: (*a*) $\lambda/D = 4.5$; (*b*) $\lambda/D = 12$.

frequency in the spanwise directions. This three-dimensional frequency St_{3D} can be computed from the Floquet multiplier and the period of sampling (T_s) as follows: $St_{3D} = \tan^{-1}(\mathrm{Im}(\mu)/\mathrm{Re}(\mu))/2\pi T_s = 0.0253$. This frequency is considerably lower than the frequencies obtained from the two-dimensional base flow. Fully three-dimensional DNS would be required to compare this frequency with the fully saturated three-dimensional wake.

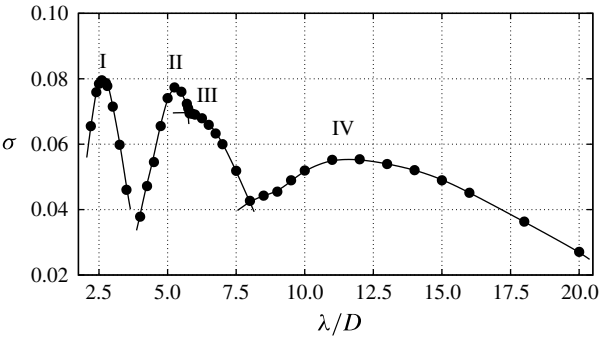

FIGURE 23. Growth rate curves for the cylinders separated by $S/D = 10$, $Re = 200$. Four distinct modes are visible, mode III being partially masked by mode II. The fastest-growing mode has a maximum growth rate at $\lambda/D = 2.6$.

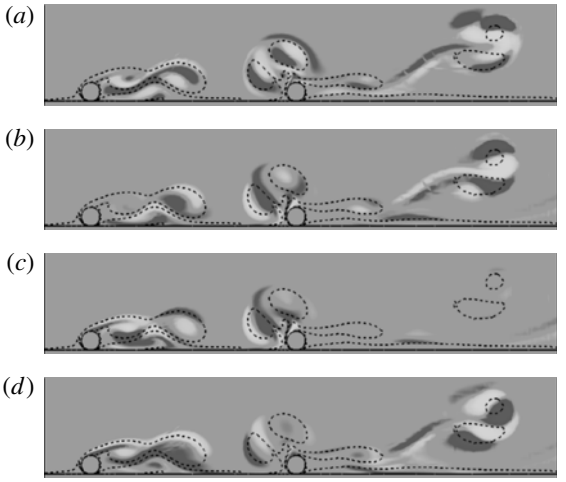

FIGURE 24. Spanwise perturbation vorticity contours for $S/D = 10$ at $Re = 200$ for the specified wavelengths. Contour shading as in figure 12: (*a*) mode I, $\lambda/D = 2.6$; (*b*) mode II, $\lambda/D = 5.5$; (*c*) mode III, $\lambda/D = 6$; (*d*) mode IV, $\lambda/D = 12$.

4.2. *Periodic base flow*

In the preceding section, the three-dimensional stability analysis was performed in the regime where the two-dimensional base flow is steady. To further explore the three-dimensional flow behaviour in the unsteady state, a Floquet stability analysis was performed at $Re = 200$ for the cylinders at the maximum separation distance of $S/D = 10$. Figure 23 shows the growth rate curves obtained by perturbing the two-dimensional base flow at different wavelengths. Four distinct modes (labelled I–IV) can be discerned, with their peaks at $\lambda/D = 2.6, 5.5, 6.0$ and 12, the fastest growing mode having the shortest wavelength. Shown in figure 24 are the spanwise perturbation contours for these modes. Inspection of the corresponding Floquet multipliers shows that modes I, III and IV are oscillating at frequencies incommensurate with the one of the base flow, leading to a quasi-periodic total flow,

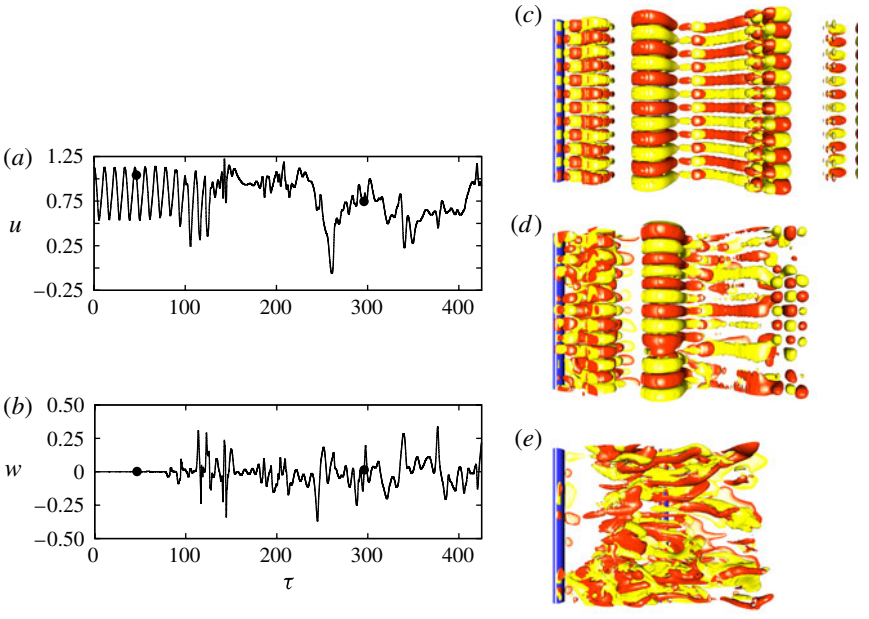

FIGURE 25. (Colour online) DNS results for the tandem cylinders sliding along a wall with $S/D = 10$ at $Re = 200$. (*a,b*) The time histories of the streamwise (u) and spanwise (w) velocity components for a location midway between the cylinders. (*c–e*) Visualizations using streamwise vorticity isosurfaces (in dark and light grey, shown in red and yellow online) viewed from above the cylinders (shown in blue online; only the upstream cylinder is visible, the downstream one being hidden by the surfaces). (*c*) Mode II with $\lambda/D = 2.4$ from linear stability analysis. (*d*) Perturbation field obtained from DNS at $\tau = 46$. (*e*) The same field at $\tau = 296$.

whereas mode II was found to be subharmonic (negative real Floquet multiplier), oscillating with a period twice that of the base flow.

5. Direct numerical simulation

At Reynolds numbers not too far above the threshold for three-dimensional transition, it appears that a number of linear modes become unstable, as shown e.g. in figure 23. To investigate the nonlinear interaction between these modes, a three-dimensional DNS was performed. A three-dimensional version of the computational code employing a Fourier expansion in the spanwise direction (Karniadakis & Triantafyllou 1992; Thompson *et al.* 1996; Ryan *et al.* 2005; Leontini *et al.* 2007) was used, with the two-dimensional solution for $S/D = 10$ and $Re = 200$ as the initial condition. A spanwise domain length of 16 cylinder diameters with 96 Fourier planes was chosen to capture the wake dynamics. Low-intensity white noise was added to trigger three-dimensional flow. The spanwise extent of the domain could contain six and three wavelengths, respectively, of the two fastest growing modes shown in figure 23. Figure 25(*a,b*) give time traces of the streamwise and spanwise velocity components at a point midway between the cylinders. Figure 25(*c*) represents the most unstable mode from linear stability analysis, using isosurfaces of positive and negative streamwise vorticity to indicate the wake structure. This should be compared with the DNS isosurfaces shown in figure 25(*d*), corresponding to $\tau = 46$, while the mode

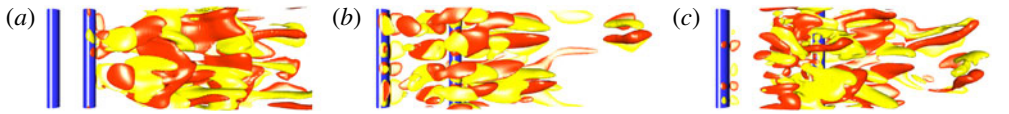

FIGURE 26. (Colour online) The final wake states at $Re = 200$ for the cylinders sliding along a wall at various spacings. These images can be compared to figure 25(*e*), where the flow eventually becomes chaotic: (*a*) $S/D = 2$; (*b*) $S/D = 5$; (*c*) $S/D = 7$.

is still undergoing exponential amplification. Figure 25(*e*) shows the complex nature of the wake at a later time ($\tau = 296$), after the wake has become highly nonlinear. As indicated above, in this state even the remnants of periodicity in the u velocity component are lost. Also, there does not appear to be a clearly dominant spanwise wavelength. Hence, the flow shows signs of a rapid transition to a chaotic state.

Figure 26 shows similar visualizations of the wake for tandem cylinders with $S/D = 2, 5$ and 7 at $Re = 200$. Starting from the respective two-dimensional solutions, the simulations were run for approximately 300 time units. For this set of simulations, the spanwise distance was set to eight cylinder diameters. For $S/D = 2$, the flow is three-dimensional and unsteady, and the long-wavelength instability is the dominant three-dimensional mode, while for $S/D = 5$ and 7, the final wake state is chaotic, similar to that observed in figure 25(*e*). In any case, the two-dimensional base flow is clearly no longer an adequate model of the real flow in this regime.

6. Conclusions

The flow past two tandem cylinders sliding along a wall has been investigated via stability analyses and limited DNS. Two-dimensional calculations were used to investigate the transition from two-dimensional steady to two-dimensional unsteady flow, when the Reynolds number is increased, as a function of the cylinder spacing. Steady flow involves multiple recirculation zones, with complicated streamline patterns arising in the gap between the cylinders for intermediate spacings. For very small and very large spacings, both steady and unsteady wakes resemble those of a single sliding body. Whereas at low Reynolds numbers in the unsteady regime, the wakes behind both cylinders oscillate at the same frequency, for larger Re an intermediate spacing range exists, where a period doubling is observed. This can be explained by a feedback mechanism, where the vortex shed from the first cylinder impacting on the second one triggers shedding of a new vortex from the first cylinder at slightly different conditions. The same phenomenon is known to occur in flow around elongated bluff bodies, where vortices are shed from both the leading and trailing edges. Of some interest, there is a stark difference between the flow dynamics of tandem cylinders placed in a free stream and tandem cylinders very close to a wall. The presence of the wall reduces the strong narrow-band absolute instability of the two-sided shedding, which, for cylinders in a free stream without wall, enables the dynamics of the upstream and downstream wakes to be at least partially independent. For the case studied here, the wake is one-sided due to the presence of the wall. The instability is not as strong, and it is receptive over a broader frequency range. Hence, the two wakes are always locked for the entire Reynolds number and separation ranges examined in this paper.

Three-dimensional stability analysis of the two-dimensional flows showed that, for all parameter combinations, the flow becomes unstable at Reynolds number well below

the threshold for unsteadiness in two dimensions. Again, for vanishing and very large cylinder separations, the unstable modes are similar to those found previously for a single sliding cylinder. In an intermediate spacing range around 5–6 cylinder diameters, a sequence of alternating regimes of three-dimensional instability and stability is observed for increasing Reynolds numbers. Whereas outside this interval the unstable three-dimensional modes are steady, the second transition within part of this range occurs through the amplification of an unsteady three-dimensional mode. Three-dimensional instability persists at higher Reynolds numbers, where the two-dimensional base flow is periodic. A Floquet stability analysis at $Re = 200$ for a large cylinder separation revealed the existence of at least four unstable modes at various wavelengths and frequencies. DNS of this flow with a spanwise domain size allowing for the growth of several of these modes showed their nonlinear interaction, leading rapidly to a disordered chaotic state.

The fact that the first transition of flow around tandem cylinders sliding along a wall involves three-dimensional steady modes, makes the results from the analysis of the transition from steady to unsteady two-dimensional flow appear less relevant for the description of realistic flows in this configuration. A similar situation was previously encountered in the study of the transitions of the wake of an isolated circular cylinder. The characteristics of the three-dimensional mode B were determined through a Floquet stability analysis of the two-dimensional periodic flow (Barkley & Henderson 1996), even though in reality the wake is already highly three-dimensional when mode B is first observed. In that case, although the critical Reynolds number is overpredicted, the predicted wavelength and spatiotemporal symmetry of mode B carry across to the real flow. For the sliding tandem cylinders examined here, the onset of three-dimensional flow is likely to alter the critical Reynolds numbers for the unsteady transition. Other observed characteristics, such as Strouhal numbers and average two-dimensional flow structures, may nevertheless remain at least roughly similar to the prediction obtained from a two-dimensional base flow. The full analysis of the unsteady transition for three-dimensional wakes is a substantial computational problem, and will form the basis of a future study.

Acknowledgements

The support from Australian Research Council Discovery Grants DP0877327, DP110100434 and DP0877517 and computing time from the National Computational Infrastructure (NCI), Victorian Life Sciences Computation Initiative (VLSCI) and Monash Sungrid are gratefully acknowledged. A.R. also acknowledges the support of a Monash University Departmental Postgraduate Scholarship.

REFERENCES

BARKLEY, D. & HENDERSON, R. D. 1996 Three-dimensional Floquet stability analysis of the wake of a circular cylinder. *J. Fluid Mech.* **322**, 215–241.

BHATTACHARYYA, S. & DHINAKARAN, S. 2008 Vortex shedding in shear flow past tandem square cylinders in the vicinity of a plane wall. *J. Fluids Struct.* **24**, 400–417.

BIERMANN, D. & HERRNSTEIN, W. H. 1933 The interference of struts in various combinations. Tech. Rep. 468. National Advisory Committee for Aeronautics.

BLACKBURN, H. M. & LOPEZ, J. M. 2003 On three-dimensional quasi-periodic Floquet instabilities of two-dimensional bluff body wakes. *Phys. Fluids* **15**, L57–L60.

CARMO, B. S., MENEGHINI, J. R. & SHERWIN, S. J. 2010 Secondary instabilities in the flow around two circular cylinders in tandem. *J. Fluid Mech.* **644**, 395–431.

CARMO, B. S., SHERWIN, S. J., BEARMAN, P. W. & WILLDEN, R. H. J. 2008 Wake transition in the flow around two circular cylinders in staggered arrangements. *J. Fluid Mech.* **597**, 1–29.

CHORIN, A. J. 1968 Numerical solution of the Navier–Stokes equations. *Maths Comput.* **22**, 745–762.

DENG, J., REN, A.-L., ZOU, J.-F. & SHAO, X.-M. 2006 Three-dimensional flow around two circular cylinders in tandem arrangement. *Fluid Dyn. Res.* **38**, 386–404.

DIDIER, E. 2007 Simulation de l'écoulement autour de deux cylindres en tandem. *C. R. Mécanique* **335**, 696–701.

ELSTON, J. R., BLACKBURN, H. M. & SHERIDAN, J. 2006 The primary and secondary instabilities of flow generated by an oscillating circular cylinder. *J. Fluid Mech.* **550**, 359–389.

GRIFFITH, M. D., LEWEKE, T., THOMPSON, M. C. & HOURIGAN, K. 2009 Pulsatile flow in stenotic geometries: flow behaviour and stability. *J. Fluid Mech.* **622**, 291–320.

HARICHANDAN, A. B. & ROY, A. 2010 Numerical investigation of low Reynolds number flow past two and three circular cylinders using unstructured grid CFR scheme. *Intl J. Heat Fluid Flow* **31**, 154–171.

HARICHANDAN, A. B. & ROY, A. 2012 Numerical investigation of flow past single and tandem cylindrical bodies in the vicinity of a plane wall. *J. Fluids Struct.* **33**, 19–43.

HENDERSON, R. D. 1997 Non-linear dynamics and pattern formation in turbulent wake transition. *J. Fluid Mech.* **352**, 65–112.

HOURIGAN, K., THOMPSON, M. C. & TAN, B. T. 2001 Self-sustained oscillations in flows around long flat plates. *J. Fluids Struct.* **15**, 387–398.

HUANG, W.-X. & SUNG, H. J. 2007 Vortex shedding from a circular cylinder near a moving wall. *J. Fluids Struct.* **23**, 1064–1076.

IGARASHI, T. 1981 Characteristics of flow around two circular cylinders arranged in tandem. *Bull. JSME* **24**, 323–331.

KARNIADAKIS, G. E., ISRAELI, M. & ORSZAG, S. A. 1991 High-order splitting methods for the incompressible Navier–Stokes equations. *J. Comput. Phys.* **97**, 414–443.

KARNIADAKIS, G. E. & SHERWIN, S. J. 2005 *Spectral/HP Methods for Computational Fluid Dynamics*. Oxford University Press.

KARNIADAKIS, G. E. & TRIANTAFYLLOU, G. S. 1992 Three-dimensional dynamics and transition to turbulence in the wake of bluff objects. *J. Fluid Mech.* **238**, 1–30.

KEVLAHAN, N. K. R. 2007 Three-dimensional Floquet stability analysis of the wake in cylinder arrays. *J. Fluid Mech.* **592**, 79–88.

KUMAR, S. R., SJARMA, A. & AGRAWAL, A. 2008 Simulation of flow around a row of square cylinders. *J. Fluid Mech.* **606**, 369–397.

LEONTINI, J. S., THOMPSON, M. C. & HOURIGAN, K. 2007 Three-dimensional transition in the wake of a transversely oscillating cylinder. *J. Fluid Mech.* **577**, 79–104.

LIANG, C., PAPAPDAKIS, G. & LUO, X. 2008 Effect of tube spacing on the vortex shedding characteristics of laminar flow past an inline tube array: a numerical study. *Comput. Fluids* **38**, 950–964.

MAHIR, N. 2009 Three-dimensional flow around a square cylinder near a wall. *Ocean Engng* **36**, 357–367.

MAMUN, C. K. & TUCKERMAN, L. S. 1995 Asymmetry and Hopf-bifurcation in spherical Couette flow. *Phys. Fluids* **7**, 80–91.

MENEGHINI, J. R., SALTARA, F., SIQUEIRA, C. L. R. & FERRARI, J. A. 2001 Numerical simulation of flow interference between two circular cylinders in tandem and side-by-side arrangements.
J. Fluids Struct. **15**, 327–350.

MITTAL, R & BALACHANDAR, S 1995 Generation of streamwise vortical structures in bluff body wakes. *Phys. Rev. Lett.* **75**, 1300–1303.

MITTAL, S, KUMAR, V & RAGHUVANSHI, A 1997 Unsteady incompressible flow past two cylinders in tandem and staggered arrangements. *Intl J. Numer. Meth. Fluids* **25**, 1315–1344.

MIZUSHIMAA, J. & SUEHIRO, N. 2005 Instability and transition of flow past two tandem circular cylinders. *Phys. Fluids* **17**, 104107.

MUSSA, A., ASINARI, P. & LUO, L.-S. 2009 Lattice Boltzmann simulations of 2D laminar flows past two tandem cylinders. *J. Comput. Phys.* **228**, 983–999.

NORBERG, C 2003 Fluctuating lift on a circular cylinder: review and new measurements. *J. Fluids Struct.* **17**, 57–96.

PAPAIOANNOU, G V, YUE, D K P, TRIANTAFYLLOU, M S & KARNIADAKIS, G E 2005 Three-dimensional flow around two circular cylinders in tandem arrangement. *J. Fluid Mech.* **558**, 387–413.

RAO, A., PASSAGGIA, P.-Y., BOLNOT, H., THOMPSON, M. C., LEWEKE, T. & HOURIGAN, K. 2012 Transition to chaos in the wake of a rolling sphere. *J. Fluid Mech.* **695**, 135–148.

RAO, A, STEWART, B E, THOMPSON, M C, LEWEKE, T & HOURIGAN, K 2011 Flows past rotating cylinders next to a wall. *J. Fluids Struct.* **27**, 668–679.

RYAN, K, THOMPSON, M C & HOURIGAN, K 2005 Three-dimensional transition in the wake of bluff elongated cylinders. *J. Fluid Mech.* **538**, 1–29.

SEWATKAR, C M, PATEL, R, SHARMA, A & AGRAWAL, A 2012 Flow around six in-line square cylinders. *J. Fluid Mech.* **710**, 195–233.

SHEARD, G J 2011 Wake stability features behind a square cylinder: focus on small incidence angles. *J. Fluids Struct.* **27**, 734–742.

SHEARD, G. J., FITZGERALD, M. J. & RYAN, K. 2009 Cylinders with square cross-section: wake instabilities with incidence angle variation. *J. Fluid Mech.* **630**, 43–69.

SHEARD, G. J., THOMPSON, M. C. & HOURIGAN, K. 2003 From spheres to circular cylinders: the stability and flow structures of bluff ring wakes. *J. Fluid Mech.* **492**, 147–180.

SHEARD, G. J., THOMPSON, M. C. & HOURIGAN, K. 2005 Subharmonic mechanism of the mode C instability. *Phys. Fluids* **17**, 111702.

STEWART, B. E., HOURIGAN, K., THOMPSON, M. C. & LEWEKE, T. 2006 Flow dynamics and forces associated with a cylinder rolling along a wall. *Phys. Fluids* **18**, 111701.

STEWART, B. E., THOMPSON, M. C., LEWEKE, T. & HOURIGAN, K. 2010*a* Numerical and experimental studies of the rolling sphere wake. *J. Fluid Mech.* **643**, 137–162.

STEWART, B. E., THOMPSON, M. C., LEWEKE, T. & HOURIGAN, K. 2010*b* The wake behind a cylinder rolling on a wall at varying rotation rates. *J. Fluid Mech.* **648**, 225–256.

THOMPSON, M. C., HOURIGAN, K., CHEUNG, A. & LEWEKE, T. 2006*a* Hydrodynamics of a particle impact on a wall. *Appl. Math. Model* **30**, 1356–1369.

THOMPSON, M. C., HOURIGAN, K., RYAN, K. & SHEARD, G. J. 2006*b* Wake transition of two-dimensional cylinders and axisymmetric bluff bodies. *J. Fluids Struct.* **22**, 793–806.

THOMPSON, M. C., HOURIGAN, K. & SHERIDAN, J. 1996 Three-dimensional instabilities in the wake of a circular cylinder. *Exp. Therm. Fluid Sci.* **12**, 190–196.

THOMPSON, M. C., LEWEKE, T. & HOURIGAN, K. 2007 Sphere–wall collisions: vortex dynamics and stability. *J. Fluid Mech.* **575**, 121–148.

THOMPSON, M. C., LEWEKE, T. & WILLIAMSON, C. H. K. 2001 The physical mechanism of transition in bluff body wakes. *J. Fluids Struct.* **15**, 607–616.

WILLIAMSON, C. H. K. 1988 The existence of two stages in the transition to three-dimensionality of a cylinder wake. *Phys. Fluids* **31**, 3165–3168.

WILLIAMSON, C. H. K. 1996 Vortex dynamics in the cylinder wake. *Annu. Rev. Fluid Mech.* **28**, 477–539.

XU, G. & ZHOU, Y. 2004 Strouhal numbers in the wake of two inline cylinders. *Exp. Fluids* **37**, 248–256.

ZDRAVKOVICH, M. M. 1987 The effects of interference between circular cylinders in cross flow. *J. Fluids Struct.* **1**, 239–261.

ZENG, L., BALACHANDAR, S. & FISCHER, P. 2005 Wall-induced forces on a rigid sphere at finite Reynolds number. *J. Fluid Mech.* **536**, 1–25.

ZHANG, H. Q., NOACK, B. R., KÖNIG, M. & ECKELMANN, H. 1995 On the transition of the cylinder wake. *Phys. Fluids* **7**, 779–793.

ZHOU, Y. & YIU, M. W. 2005 Flow structure, momentum and heat transport in a two-tandem-cylinder wake. *J. Fluid Mech.* **548**, 17–48.